Available online at www.sciencedirect.com

ScienceDirect

Journal of Hydro-environment Research 8 (2014) 396–409

Journal of Hydro-environment Research

www.elsevier.com/locate/jher

Research paper

Simulation of flow in compound open-channel using a discontinuous Galerkin finite-element method with Smagorinsky turbulence closure

Chien Pham Van [a,b,*], Eric Deleersnijder [c,d], Didier Bousmar [e], Sandra Soares-Frazão [a]

[a] Institute of Mechanics, Materials and Civil Engineering (iMMC), Université Catholique de Louvain, Place du Levant 1, B-1348 Louvain-la-Neuve, Belgium
[b] Faculty of Hydrology and Water Resource, Water Resources University, Tayson 175, Dongda District, Hanoi, Viet Nam
[c] Institute of Mechanics, Materials and Civil Engineering (iMMC), Université Catholique de Louvain, Avenue Georges Lemaître 4, B-1348 Louvain-la-Neuve, Belgium
[d] Georges Lemaître Centre for Earth and Climate Research (TECLIM), Earth and Life Institute (ELI), Université Catholique de Louvain, Chemin du Cyclotron 2, B-1348 Louvain-la-Neuve, Belgium
[e] Hydraulic Research Laboratory, Service Public de Wallonie, Rue de l'Abattoir 164, 6200 Châtelet, Belgium

Received 30 April 2013; revised 4 April 2014; accepted 5 April 2014
Available online 18 April 2014

Abstract

The small-scale spatial variability of eddy viscosity which is characteristic for the turbulent shear stress in compound open-channel flows was studied and investigated in this paper. Different options including a constant value, zero-equation, one-equation, two-equation, and Smagorinsky turbulence models for parameterizing the eddy viscosity were developed in the framework of the discontinuous Galerkin finite-element SLIM model and applied for presenting the complex velocity profile in two different experimental data sets of laboratory flumes. A very good qualitative agreement was achieved between numerical results and measurement data for both velocity and flow depth of all experimental data sets in general. In addition, the calculation results showed that the turbulent Smagorinsky empiricism allowed a better presentation of non-uniform velocity in the floodplain and transition regions between plain and main channels than the others in all calculated cases. This empiricism predicted a very close variation of eddy viscosity in comparison with the results calculated by the depth-averaged Reynolds' stress and the lateral gradient of longitudinal velocity. The eddy viscosity varies significantly in the channel section; in particular the small values often occurred around the middle location of floodplains and the central location of the main channel while the large values appeared in the transition regions, presenting different minimum and maximum values of eddy viscosity in each flow region. The effects of eddy viscosity variation on lateral distribution of velocity profile were also investigated and discussed.

Keywords: Eddy viscosity; Smagorinsky turbulent model; Finite-element model; Velocity distribution; Compound open-channel

1. Introduction

Flows in open-channels with compound cross-sections are very dynamic and complex due to the transverse transfer of momentum between the fast flow in the main channel and the adjacent slower flow in the floodplains (Sellin, 1964; Keller and Rodi, 1988). This transfer is driven by the turbulent shear stresses generated at the interface between the main channel and the floodplain. Ervine et al. (2000) stated that these turbulent shear stresses are the main reasons for the

* Corresponding author. Institute of Mechanics, Materials and Civil Engineering (iMMC), Université Catholique de Louvain, Place du Levant 1, B-1348 Louvain-la-Neuve, Belgium. Tel.: +32 10 47 21 24; fax: +32 10 47 21 79.
E-mail addresses: chien.phamvan@uclouvain.be, chienyonsei@gmail.com (C. Pham Van).

http://dx.doi.org/10.1016/j.jher.2014.04.002

existence of non-zero transverse velocity even in straight compound open-channels. The ratio of this transverse velocity to the longitudinal velocity component can vary in a typical range of 2–4%. Using direct numerical simulation (DNS), Joung and Choi (2008) found a ratio of about 5% for a turbulent flow in a rectangular compound open-channel. As described by Shiono and Knight (1991), the resulting flow from these turbulent shear stresses presents three-dimensional features, i.e. effects of bed-generated turbulence and lateral shear turbulence when the ratio between the water-depth in the floodplain and in the main channel becomes sufficiently low.

Modeling of these turbulent shear stresses is usually achieved by means of the concept of eddy viscosity that is applied both in three-dimensional (3D) models and in two-dimensional (2D) depth-averaged models. For large-rivers applications, 2D models are widely used as they allow for reasonable computational times, especially for long-term simulations. However, these 2D models need to be validated first using detailed data that can only be obtained from laboratory compound open-channels experiments. In this case, since the vertical scale (typically by the water depth) is still much smaller than the lateral scale characterized by the channel width, the flow field can be also treated as two-dimensional depth-averaged. In that depth-averaged framework, the eddy viscosity ν_t can be modeled with different levels of complexity. For example, Vreugdenhil and Wijbenga (1982) used a constant value of ν_t all over the flow to compute the lateral momentum exchanges in compound channels. Rajaratnam and Ahmadi (1981) used experimental data and a theoretical analysis to study the variation of eddy viscosity in the mixing region between main channel and floodplain. They reported that the eddy viscosity depends on the channel geometry, the lateral distribution of velocity, and the boundary shear stress. However, the proposed expression is difficult to apply due to the uncertainty in the determination of the mixing length region. A simpler expression was provided by Wormleaton (1988) who used a length scale related to the width of the shear layer and the velocity difference across the shear layer to determine the lateral eddy viscosity in the case of shear layer driven turbulence within a compound channel.

Another widely used approach consists of modeling eddy viscosity using an expression based on a non-dimensional eddy viscosity parameter λ, the shear velocity, and the flow depth (Wark et al., 1990; Darby and Thorne, 1996), under the form $\nu_t = \lambda u_* H$ which is known as the zero-equation turbulent model for eddy viscosity in the literature. An interesting summary of λ values is illustrated in Ervine et al. (2000), who report the value $\lambda = 0.16$ that is often used for laboratory flumes and real river applications. Using this zero-equation turbulent model approach, other authors proposed to determine different constant values of λ in each flow region, i.e. the floodplains and the main channel (Pasche and Evers, 1985; Zeng et al., 2012). This latter approach was also used by Vionnet et al. (2004) who applied the one-dimensional lateral distribution method (LDM) for initially estimating the eddy viscosity coefficient ν_t in vegetated floodplains and in the main channel. Then, they stated that a value of $\lambda = 0.071$ determined with the LDM for the main channel region could be uniformly used for both main and floodplain channel in their Telemac-2D simulations on vegetated floodplain. In addition, based on the best fit with data from laboratory experiments, Sung-Uk and Pham Van (2010) showed that the values of $\lambda = 0.061$ and 0.16 could be used for emergent vegetation floodplains and for the main channel, respectively, in a study related to the impact of floodplain vegetation on the morphological change of straight compound open-channel. The zero-equation turbulent model for eddy viscosity is, however, limited to straight open-channel calculations in which the overbank flows are near uniform.

Recently, Zeng et al. (2012) estimated the eddy viscosity ν_t based on the ratio of the depth-averaged Reynolds' stress and the lateral gradient of longitudinal velocity. In such an approach, the velocity distribution over the channel width is the key hydraulic parameter for the determination of the eddy viscosity that in turn will affect this velocity distribution in the calculations. In addition, the cross-section must be divided into several sub-domains (e.g. floodplain, main channel, transition region between plain and main channels) in the case of compound channels. Thus, this approach is very difficult to apply in the real situations since the natural channel bed could be changed arbitrarily in the lateral direction, and the velocity distribution is a priori unknown.

The eddy viscosity ν_t can also be determined from the turbulent kinetic energy and its dissipation rate. This more complex approach is applied or implemented in many modeling studies of open-channel flow, in which a depth-averaged version of $k-\varepsilon$ turbulence model proposed by Rastogi and Rodi (1978) is the most commonly used in depth-averaged calculations (e.g. Keller and Rodi, 1988; Wilson et al., 2002; Kuzmin and Mierka, 2006). Further information of original development of $k-\varepsilon$ turbulence model refers in Launder and Spalding (1974). This approach is known as the two-equation model for estimating the eddy viscosity. Two transport equations involving several empirical coefficients are solved in addition to the hydrodynamic flow equations for calculating the turbulent kinetic energy (TKE) k and dissipation rate ε over the channel. Solving these additional equations can result in a significant increase in computational cost. An interesting compromise is provided by a simpler model, such as the one-equation model, which has proved its efficiency in previous studies related to compound channel flows (e.g. Smith and Takhar, 1977; Radojkovic and Djordjevic, 1985; Wilson et al., 2002; Fraselle, 2010).

Another type of approach is the one originally proposed by Smagorinsky (1963), which was originally developed to study the dynamics of the atmosphere's general circulation. This model is most commonly used for subgrid-scale shear-stress models in large-eddy simulations of homogenous and isotropic turbulent flow (Pope, 2000). It is widely applied in coastal models for parameterizing the horizontal eddy viscosity (Madsen et al., 1988; Lambrechts et al., 2008b; de Brye et al., 2010; de Brye et al., 2011, etc). In regards to smaller-scale applications such as shallow river flow, an example application of Smagorinsky turbulent model for evaluating the eddy

viscosity is presented in Nasermoaddeli and Pasche (2010) who solved the 2D depth-averaged Navier–Stoke's equations within the finite element fluvial model RMA10s for studying the undercutting and failure of non-cohesive sandy riverbanks. However, applications of this turbulence model to small-scale flows are still lacking, especially for compound open-channel flumes in the laboratory. The possibility to use such a model in compound open-channel flows is investigated here by comparing the simulation results to experimental measurements and to a selection of more classical models used in compound-channel flow simulations.

Different numerical methods exist for the simulation of open-channel flows and in particular flows in compound channels, where the accurate prediction of the velocity distribution is a key issue (Wark et al., 1990; Sung-Uk and Pham Van, 2010). Wark et al. (1990) developed a finite difference (FD) method for the simulation of the 1D lateral distribution of velocity and/or unit discharge ($q = u \times H$) estimation in a channel section. They suggested that the proposed finite difference method is suitable for river modeling. It has been applied in a wide range of applications, varying from small-scales laboratory flumes to large-scale of laboratory channels and real rivers (e.g. Sung-Uk and Pham Van, 2010; Darby and Thorne, 1996; etc). Keller and Rodi (1988) used a combined finite difference and finite volume (FV) method with a $k-\varepsilon$ model for the turbulence closure to predict the flow characteristics in the main channel and in the floodplain. Finite-element (FE) models are widely used to simulate a wide range of flows, both 2D and 3D, and present some significant advantages: they allow for (i) an accurate representation of complex topographies by using unstructured meshes and (ii) an increase in spatial resolution by using high-order reconstruction in each element (Bernard et al., 2007; Comblen et al., 2010).

In this paper, a depth-averaged Discontinuous-Galerkin (DG) finite-element model developed within the framework of the SLIM project (www.climate.be/slim) is used to simulate flows in compound channels. The DG method offers the advantage over classical finite-element models to allow for the representation of discontinuous variables, e.g. hydraulic jumps, in a more accurate way. The SLIM model solves the two-dimensional depth-averaged shallow-water equations, including depth-averaged turbulent source terms. Although this model was initially developed for modeling flows in coastal areas (Bernard et al., 2007; Lambrechts et al., 2008b), it is now more and more applied to estuaries and inland waterways (de Brye et al., 2010, 2011). This study thus aims (i) to assess the ability of the SLIM model to reproduce the complex velocity profile in compound channels and (ii) to investigate the ability of a Smagorinsky turbulent model to reproduce the depth-averaged shear-stresses arising between the main channel and the floodplain. The computed results by means of the Smagorinsky approach are compared to experimental data obtained in the compound-channel flume of the Hydraulics Laboratory at Université Catholique de Louvain (UCL, Belgium) and to results obtained by means of different turbulent closure models (e.g. constant ν_t, $\nu_t = \lambda u_* H$, the one-equation model, and the two-equation model) or from the literature.

2. Finite-element SLIM model

2.1. Governing equations

The flow characteristics, comprising the water depth and velocities are determined by solving the two-dimensional depth-averaged shallow-water equations, written in the following form:

$$\frac{\partial \eta}{\partial t} + \nabla \cdot (H\mathbf{u}) = 0, \tag{1}$$

$$\frac{\partial u}{\partial t} + \mathbf{u} \cdot (\nabla \mathbf{u}) + g\nabla \eta = -\frac{gn^2 \|\mathbf{u}\|}{H^{4/3}}\mathbf{u} + \frac{1}{H}\nabla \cdot [H\nu_t(\nabla \mathbf{u})], \tag{2}$$

where t is the time and ∇ is the del operator; $H = \eta + h$ is the total water depth in which h and η are the water depth below and above the reference level, respectively; g is the gravitational acceleration, ν_t is the horizontal eddy viscosity; $\mathbf{u} = (u, v)$ is the depth-averaged horizontal velocity vector that represents respectively the longitudinal and transverse velocity components; and n is the Manning coefficient representative for the bottom friction.

2.2. Eddy viscosity

The horizontal eddy viscosity ν_t can be evaluated in different ways in the SLIM model. The simplest choice consists in using a constant value of ν_t over the whole computational domain. Another option consists in using constant values that differ in the main channel and in the floodplains.

A variable eddy viscosity can be obtained using the $\nu_t = \lambda u_* H$ model, in which the shear velocity u_* is calculated as $u_*^2 = c_f u^2$ with c_f being a coefficient obtained from Manning's formula ($c_f = gn^2 H^{-1/3}$). The key parameter in this approach is the dimensionless eddy viscosity parameter λ, for which indicative values are available from the literature. It should be noted that both uniform and spatially variable values of λ can be used in a cross-section of compound open-channels. For instance, Fraselle (2010) used a constant value of 0.21 for λ to reproduce the lateral distribution of velocity in a compound laboratory flume using the finite element Telemac-2D software while Zeng et al. (2012) used $\lambda = 0.47$ and 0.16 for the floodplains and the main channel, respectively.

A third approach that can be used in SLIM is to calculate the eddy viscosity using the Smagorinsky turbulent model (Smagorinsky, 1963) in which ν_t is expressed in terms of the magnitude of the resolved rate-of-strain or the depth-averaged velocity gradients, the mesh size Δ, and a non-dimensional coefficient C_s.

$$\nu_t = (C_s\Delta)^2 \sqrt{2\left(\frac{\partial u}{\partial x}\right)^2 + 2\left(\frac{\partial v}{\partial y}\right)^2 + \left(\frac{\partial u}{\partial y} + \frac{\partial v}{\partial x}\right)^2}. \tag{3}$$

Madsen et al. (1988) reported that the coefficient C_s ranges from 0.4 to 0.8 for depth-averaged modeling applications while Nasermoaddeli and Pasche (2010) showed that this coefficient varies in a range between 0.065 and 0.23. Based on equation (3), it is clearly seen that the value of the non-dimensional coefficient C_s depends on the mesh size. In the present study, the coefficient (C_s) is considered as a modeling parameter and its value will be determined based on the best fit to the measurement data of flow depth and velocity profiles.

Another option for estimating the eddy viscosity is that ν_t could be calculated by using the one-equation model, based on the following considerations. The eddy viscosity is estimated as

$$\nu_t = C_\mu \frac{k^2}{\varepsilon}, \tag{4}$$

where k and ε are respectively the kinetic energy turbulence and its dissipation rate; $C_\mu = 0.09$ is an empirical constant whose value is proposed based on flow experiments (Launder and Spalding, 1974; Rastogi and Rodi, 1978; Rodi, 1980).

According to Nadaoka and Yagi (1998) who developed a computational model known as the SDS-2DH model to simulate shallow water turbulent flows, the TKE is calculated by the following energy-transport equation

$$\frac{\partial k}{\partial t} + \mathbf{u}\cdot(\nabla k) = \nabla\cdot\left[\frac{\nu_t}{\sigma_k}(\nabla k)\right] + P_h - \varepsilon, \tag{5}$$

where σ_k is an empirical constant and its value adopted from Launder and Spalding (1974) is $\sigma_k = 1.0$; the P_h term corresponds to the turbulent kinetic energy production due to the interaction between the turbulent shear stress and the depth-averaged velocity gradient:

$$P_h = \nu_t\left[2\left(\frac{\partial u}{\partial x}\right)^2 + 2\left(\frac{\partial v}{\partial y}\right)^2 + \left(\frac{\partial u}{\partial y} + \frac{\partial v}{\partial x}\right)^2\right]. \tag{6}$$

The energy dissipation rate ε is evaluated by the length scale (l_d) and kinetic energy of turbulence (Nadaoka and Yagi, 1998).

$$\varepsilon = C_d \frac{k^{3/2}}{l_d}, \tag{7}$$

where $C_d = 0.17$ is a constant (Rodi, 1980; Nadaoka and Yagi, 1998). The turbulence length-scale l_d is assumed to be proportional to the flow depth as $l_d = \xi H$, with $\xi = 0.1$ as suggested by Nadaoka and Yagi (1998) for determining the turbulence length-scale l_d of the flow in shallow water.

In the last option, the eddy viscosity is estimated using a two-equation model (k–ε model), under the form of equation (4). The turbulence kinetic energy and its dissipation rate are determined by solving two energy-transport equations (Rastogi and Rodi, 1978).

$$\frac{\partial k}{\partial t} + \mathbf{u}\cdot(\nabla k) = \nabla\cdot\left[\frac{\nu_t}{\sigma_k}(\nabla k)\right] + P_h + P_{kv} - \gamma k, \tag{8}$$

$$\frac{\partial \varepsilon}{\partial t} + \nabla\cdot(\mathbf{u}\varepsilon) = \nabla\cdot\left[\frac{\nu_t}{\sigma_\varepsilon}(\nabla \varepsilon)\right] + c_{1\varepsilon}\gamma P_h - c_{2\varepsilon}\gamma\varepsilon + P_{\varepsilon v}, \tag{9}$$

where $\sigma_\varepsilon = 1.3$, $c_{1\varepsilon} = 1.44$, and $c_{2\varepsilon} = 1.92$ are constants; $\gamma = \varepsilon/k$ is the auxiliary parameter (Kuzmin and Mierka, 2006), P_{vk} and $P_{v\varepsilon}$ are source terms which express the turbulent kinetic energy production due to the bed friction and they are related to the shear velocity (Rastogi and Rodi, 1978),

$$P_{kv} = \frac{1}{\sqrt{c_f}}\frac{u_*^3}{H} \quad \text{and} \quad P_{\varepsilon v} = \frac{1}{\sqrt{e_* \sigma_t}}\left(\frac{c_{2\varepsilon}}{c_f^{3/4}}\sqrt{c_\mu}\right)\frac{u_*^4}{H^2}, \tag{10}$$

with $e_* = 0.15$ and $\sigma_t = 0.5$.

2.3. Finite element implementation

The depth-averaged shallow water equations (1) and (2) and the energy-transport equations, i.e. (5), (8), and (9) are solved in SLIM using a DG finite element method (DG-FEM) that is described in detail in Comblen et al. (2010), de Brye et al. (2010), and Kärnä et al. (2011). Thus, only general information about the finite element implementation are provided herein. The computational domain is discretized into a series of triangular elements. The governing equations are multiplied by test functions and then integrated by parts over each element, resulting in element-wise surface and contour integral terms for the spatial operators. Using linear shape function over each element or triangle (Fig. 1), discontinuities appear between the values of the variables at the interface between two adjacent elements, resulting in the use of approximate Riemann solver for the fluxes between computational cells (Comblen et al., 2010). The linear reconstruction implies a second-order spatial accuracy. Temporal integration is then achieved using a second-order diagonally implicit Runge–Kutta method.

2.4. Boundary conditions

At the inlet section of the channel flume, a constant water discharge is provided in each flow region, i.e. main channel and floodplain, as the upstream boundary condition. This discharge is simply estimated using the ratio of each region area to the total area of channel section. A constant water level

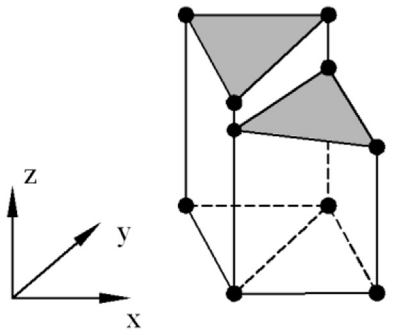

Fig. 1. Schematic illustration for the nodes in framework of DG-FEM.

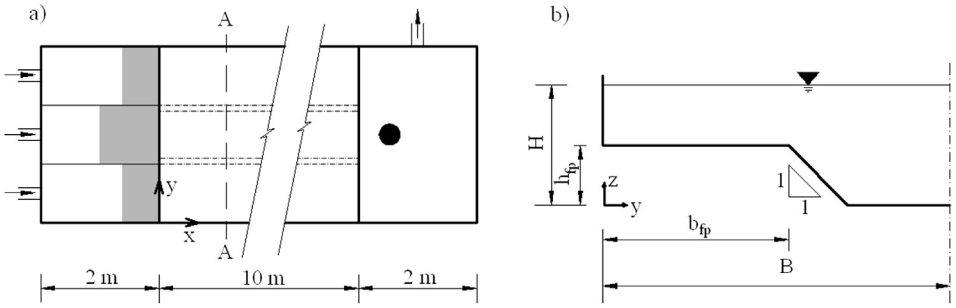

Fig. 2. Experimental set-up in the Hydraulic Laboratory of the UCL: a) plan view and b) a haft of cross-section A–A.

($\eta = H - h$) which is calculated from the experimental flow depth H and the water depth h below the reference level is prescribed at the downstream end of the channel flume. In addition, the normal gradient of velocity is also set equal to zero at the downstream boundary in order to eliminate the surface integral terms which result from integration by parts in the finite element framework. Free-slip conditions are imposed at the channel walls because (i) the influence of channel wall (or boundary layers) is limited to the region close to the side wall, (ii) a detailed resolution of the near-wall flow is not the main purpose of the study since a detailed resolution of these near-wall features would result in a too heavy computational cost, and (iii) to avoid the zero value of eddy viscosity in the calculations at the wall boundary.

In the case of using two-equation model for evaluating the eddy viscosity, the turbulent kinetic energy k and dissipation rate ε must be provided, beside the abovementioned flow conditions. At the upstream boundary, we prescribe $k = c_{bc}|u|^2$ and $\varepsilon = c_\mu k^{3/2}/l_0$ where c_{bc} is an empirical constant whose value varies in a range between 0.003 and 0.01 according to Kuzmin and Mierka (2006) and l_0 is the mixing length that is taken the same as the value of turbulence length-scale of the flow in shallow water proposed by Nadaoka and Yagi (1998). In this study, $c_{bc} = 0.02$ is applied to obtain a similar magnitude of eddy viscosity as with the first three models. At the downstream boundary, the normal gradient of turbulence kinetic energy and dissipation rate are set equal to zero ($\mathbf{n}\cdot\nabla k = 0$ and $\mathbf{n}\cdot\nabla\varepsilon = 0$). Similarly, $k = c_{bc}|u|^2$ and $\mathbf{n}\cdot\nabla k = 0$ are provided at upstream and downstream boundaries, respectively when the one-equation model is applied to estimate the eddy viscosity.

3. Experimental data

Two experimental data sets from different sources are used for calibrating the modeling parameters and for investigating the distribution of eddy viscosity in this study. The first one was performed at the Hydraulics Laboratory of the Université Catholique de Louvain (Fraselle, 2010) while the other one was reported by Zeng et al. (2012). The two data sets are briefly presented in the next sections, while detailed results will be shown in Sections 4 and 5.

Table 1
Channel geometry and hydraulic parameters in experimental set-ups.

No.	Q (m^3/s)	H (cm)	h_{fp} (cm)	b_{fp} (m)	B (m)	S_0	R (m)	U_0 (m/s)
1	0.015	6.60	5.08	0.4050	0.605	0.0019	0.028	0.415
2	0.020	7.27	5.08	0.4050	0.605	0.0019	0.034	0.452
3	0.0172	9.72	6.54	0.4456	0.609	0.00123	0.042	0.311

3.1. Experimental data set n° 1

The flow experiments, described in details in Fraselle (2010), were performed in a compound channel flume with glass walls whose total length was equal to 14.0 m (Fig. 2a). This length consisted of a 10.0 m long measurement section, a 2.0 m long inlet tank, and a 2.0 m outlet zone. The section in the inlet tank was divided into three subsections (right and left floodplains, and main channel), each one being supplied by a pump in order to allow for different inlet discharges in each subsection. The discharge measurement was operated by electromagnetic flow-meters. The outlet zone was used to control the downstream water level by means of an adjustable weir in order to achieve a uniform flow. For example, at a given discharge, the uniform flow was obtained by adjusting the downstream water level until the longitudinal water profile in the channel was parallel to the channel bed. The flow depth was measured along the channel by means of an ultrasonic probe (Keyence ud-20) mounted on the automatic positioning device while the velocity field was determined using a Pitot tube device. Detailed information about the flume and the measurement process can be found in Bousmar et al. (2005) and Fraselle (2010). Additional characteristics of the flume channel are summarized in Table 1, in which the half width of the channel B equals 0.605 m; the width b_{fp} and the height h_{fp} of the floodplain region are 0.405 and 0.0508 m, respectively (Fig. 2b). The bed slope S_0 was 0.0019. Main channel and floodplain beds are made from coated plywood, with a global Manning roughness coefficient in the range 0.010.

Two different total discharges were considered: $Q = 0.015$ m^3/s and $Q = 0.020$ m^3/s. The uniform flow depths and other relevant hydraulic parameters corresponding to these discharges are summarized in Table 1 (No. 1 and No. 2). Notice that the U_0 is the cross-sectional average velocity and the hydraulic radius R is calculated using the total area and the total wetted perimeter of the channel cross-section.

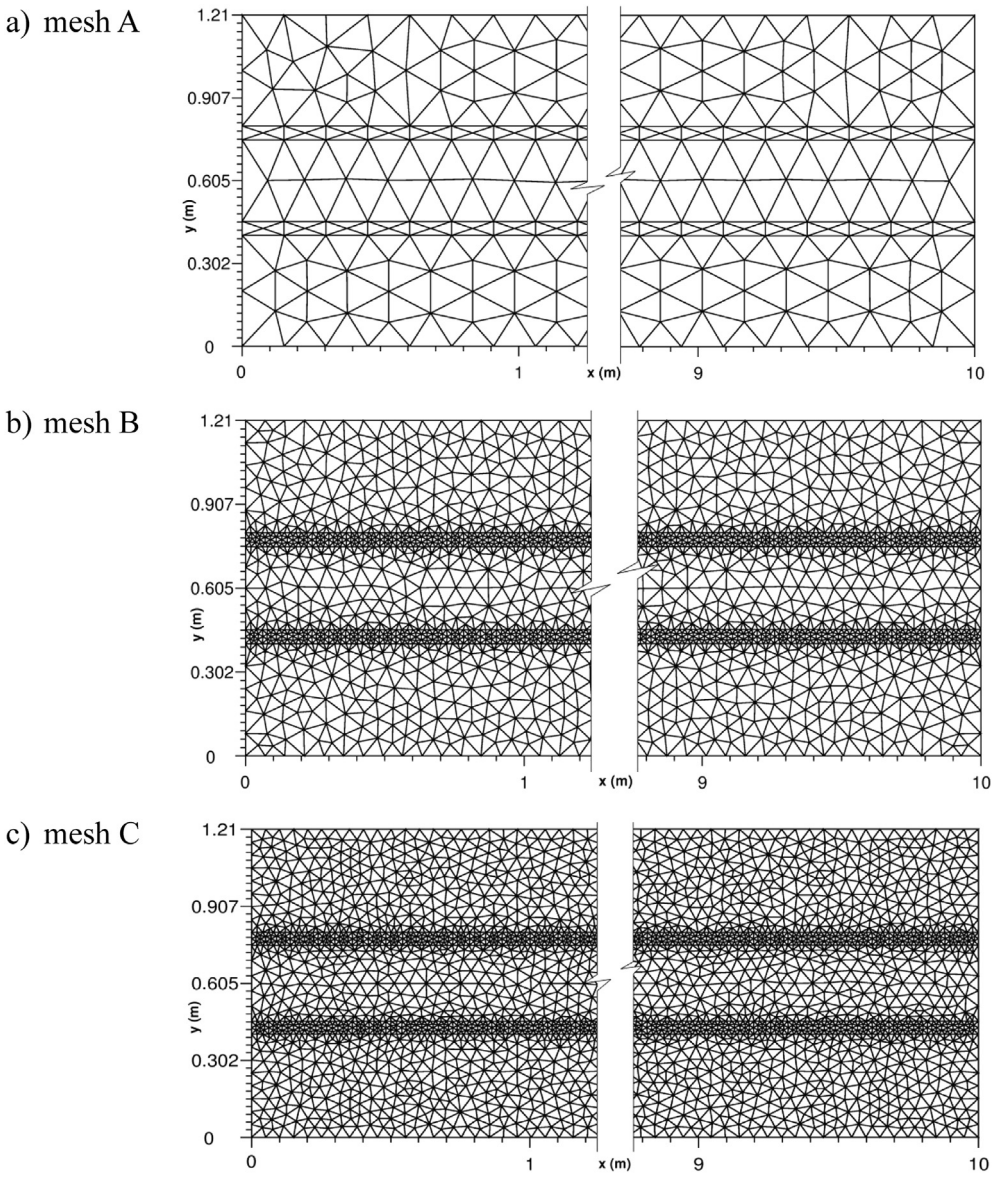

Fig. 3. Different meshes for the computational simulations.

3.2. Experimental data set n° 2

The second experimental data set was also obtained in a trapezoidal compound open-channel flume, located at $x = 2.6418$ m downstream from the inlet section, as reported by Zeng et al. (2012) and related references therein. The hydraulic parameters of this data set are listed in Table 1 (No. 3). A water discharge of 0.0172 m^3/s, corresponding to a 9.72 cm water depth was used for the measuring process. This experiment was achieved using a similar channel width as for the previous data set ($B = 0.609$ m) but a longer channel length (20 m) and a lower bed slope compared to the first one. Velocity profiles were measured using a non-intrusive 2D Laser Doppler Anemometry technique. Both instantaneous and temporal averaged velocities in transverse and longitudinal directions of the channel flume were measured over one half of the channel. From these measurement data of velocities, the eddy viscosity could be estimated based on the depth-averaged Reynolds' stresses and the lateral gradient of longitudinal velocity.

4. Numerical simulations: calibration of the models and sensitivity analysis

In this section, the results from different simulations corresponding to the first experimental data set with a discharge $Q = 0.020$ m^3/s (case No. 2 in Table 1) are presented and compared to the measurements. First, a reference simulation using the Smagorinsky model is performed for determining the Manning coefficient and the eddy viscosity coefficient C_s. Then, a sensitivity analysis of the model results to the Manning roughness coefficient, the mesh size and the turbulence closure model is carried out. The different computational meshes used in the simulations are illustrated in Fig. 3, the

Table 2
Values of parameters and calculation results for reference simulations.

#	Mesh	Eddy viscosity		Friction coefficient, n	Flow depth, H (cm)		Longitudinal velocity		
		Model	C_s		Computed	Measured	RMS error	MAE	r
1	B	Smagorinsky turbulent model	0.3873	0.006	6.73	7.27	0.094	0.079	0.996
2				0.011	7.24		0.017	0.013	0.997
3				0.016	7.58		0.061	0.054	0.991
4			0.0894	0.011	7.24		0.020	0.016	0.993
5			0.5477		7.25		0.023	0.020	0.997

choice for the reference simulation being mesh B with 16,204 computational cells or elements.

4.1. Reference simulation using Smagorinsky model

Using mesh B and the Smagorinsky model, different constant bottom frictions and constant non-dimensional coefficients C_s in the whole channel are tested to obtain the best fit with the experimental data. The value of each parameter is varied separately, whilst keeping the other one constant. The detailed computed water depth, root mean square (RMS) error of velocity, mean absolute error (MAE) of velocity, and Pearson's correlation coefficient (r) between computed and observed velocities from these trial and error simulations are shown in Table 2 while the comparison between measured and calculated velocity in the channel section is illustrated in Fig. 4.

Fig. 4a shows the results corresponding to the case using different constant roughness coefficients (e.g. 0.006, 0.011, 0.016) and a constant value of non-dimensional coefficient ($C_s = 0.3873$). It is not surprising that the flow depth increases significantly and the velocity decreases with increasing Manning friction coefficient, especially in the main channel region. The model reproduces very well the lateral distribution of velocity with the bottom friction value $n = 0.011$. The RMS error of velocity in this simulation is of about 0.017 m/s and a slightly smaller water depth is achieved in comparison with the measured value. The results appear to be less sensitive to a variation of C_s, as illustrated in Fig. 4b where different constant coefficient C_s and a constant friction ($n = 0.011$) are used. The RMS error of velocity remains close to 0.02 m/s for small and large values of the non-dimensional coefficient C_s. Finally, the values $n = 0.011$ and $C_s = 0.3873$ are selected as the reference values for further investigating separately the effects of each modeling parameter, i.e. roughness coefficient distribution, mesh size, and eddy viscosity model.

4.2. Roughness coefficient

In the reference simulation, a slight overestimation of the velocity in the floodplain region can be observed (Fig. 4b) even though the model shows the reasonable water depth and velocity in the channel in general. Several simulations with different friction coefficients in the main channel and in the floodplains are performed in order to improve the computational results. The computed water depth, RMS error of the velocity, MAE, and coefficient r obtained by using different friction coefficients in the floodplains are summarized in Table 3, in which the subscripts mc and fp refer to the main channel and floodplain, respectively. The value $n = 0.011$ is kept constant in the main channel.

As shown in Fig. 5a, the velocity in the floodplains significantly increases for decreasing bottom friction, resulting in a significant change of the flow depth in the main channel (Table 3). The best fit value is found for $n_{fp} = 0.013$ (Fig. 5b): the results improve significantly not only for the flow depth but also for the velocity distribution in the channel, and especially at the transition between main channel and floodplain. The RMS error of velocity is of about 0.0161 (<4% of cross-sectional average velocity U_0). It should be noted that

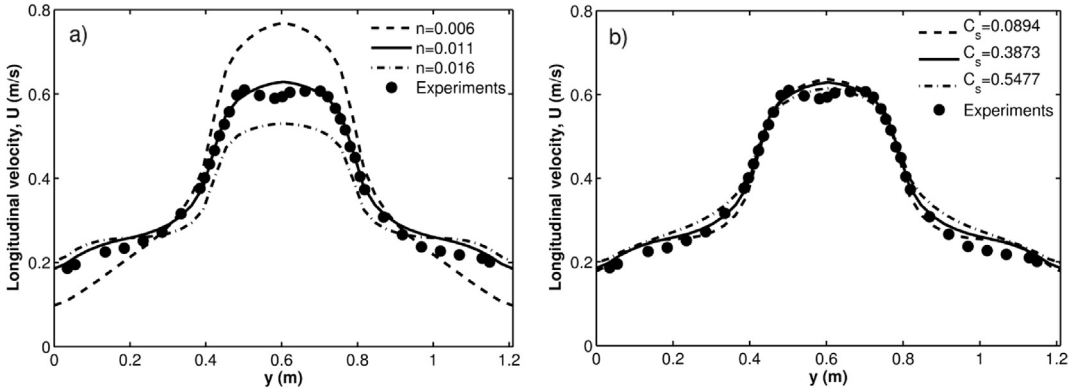

Fig. 4. Lateral distributions of velocity at: a) different friction coefficients and b) different constant parameters C_s.

Table 3
Different friction coefficient in floodplain and calculation results.

#	Mesh	Eddy viscosity		Friction coefficient		Flow depth, H (cm)		Longitudinal velocity		
		Model	C_s	n_{mc}	n_{fp}	Computed	Measured	RMS error	MAE	r
1	B	Smagorinsky turbulent model	0.3873	0.011	0.008	6.85	7.27	0.080	0.073	0.994
2					0.013	7.27		0.016	0.012	0.995
3					0.030	7.33		0.084	0.069	0.983

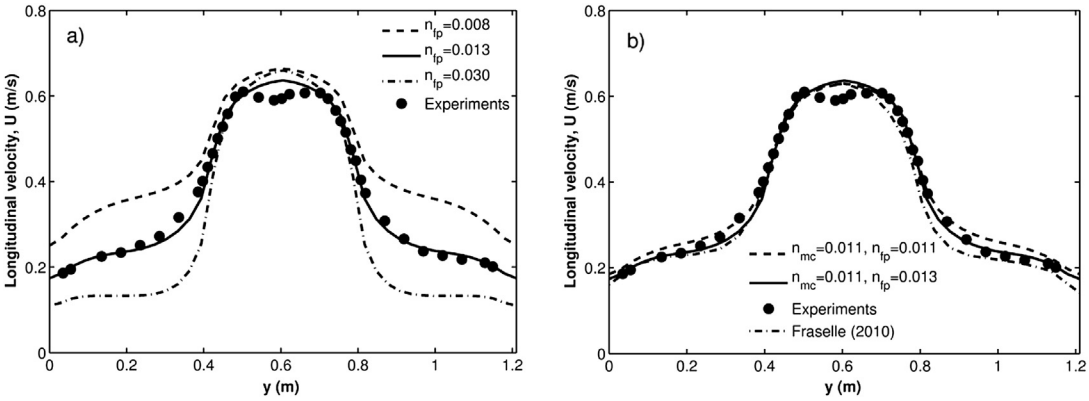

Fig. 5. Impacts of bottom coefficients on velocity profiles: a) different friction coefficient in the floodplain and b) constant and variable friction coefficients in channel.

the resulting roughness coefficients are in the expected range of values for the actual channel bed material.

Fraselle (2010) used the finite element model Telemac-2D for reproducing the depth-averaged velocity in the same experimental data set. He reported calibrated values for the bottom friction coefficients of $n_{mc} = 0.010$ and $n_{fp} = 0.014$ when using the zero-equation model for evaluating the eddy viscosity (with constant value of $\lambda = 0.21$). The calibrated Manning coefficients for the finite-element SLIM model are very similar to these latter values obtained using a different turbulence closure model and a different computational software. The slight difference can be explained by the difference in turbulence closure. The influence of the choice of the closure model will be discussed in Section 4.4.

The results obtained by Fraselle (2010) showed an underestimation of velocity in floodplain regions and in the main channel region from $y = 0.65–0.8$ m (Fig. 5b). Indeed, the results also presented nearly uniform velocity distribution in the floodplains (except in the region close to the side wall) that is not observed in the measurements. In the present study, using a Smagorinsky turbulent closure, a much better agreement with the measured velocity profile is obtained.

4.3. Mesh size

Different computational meshes (Fig. 3) were generated using the open-source mesh generation software GMSH (www.geuz.org/gmsh, described in, i.e. Lambrechts et al., 2008a; Geuzaine and Remacle, 2009). The total number of triangles (elements or cells) increases significantly from the coarse mesh A to the very fine mesh C. For instance, the coarse mesh A (Fig. 3a) has 1724 triangles corresponding to an element edge length approximately equal to 8 cm while mesh B (Fig. 3b) and mesh C (Fig. 3c) show the fine meshes,

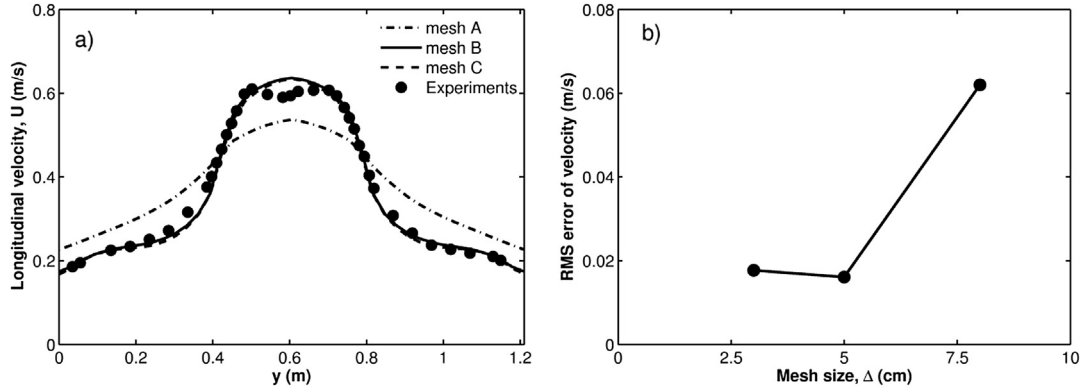

Fig. 6. Simulation results obtained by using different meshes: a) lateral distribution of velocity and b) RMS error of velocity versus the mesh size.

Table 4
Parameters value and calculation results in the case using different meshes for sensitivity analysis.

#	Eddy viscosity		Friction coefficient		Mesh	Flow depth, H (cm)		Longitudinal velocity		
	Model	C_s	n_{mc}	n_{fp}		Computed	Measured	RMS error	MAE	r
1	Smagorinsky turbulent model	0.3873	0.011	0.013	A	7.53	7.27	0.062	0.056	0.979
2					B	7.27		0.016	0.012	0.995
3					C	7.54		0.018	0.013	0.995

with 2 cm elements in the transition region and 5 cm element (mesh B) or 3 cm elements (mesh C) elsewhere. The total numbers of triangles of these fine meshes are 16,204 for mesh B and 21,204 for mesh C.

Fig. 6 shows the simulation results obtained by using the different meshes and the optimized values of the Manning coefficient ($n_{mc} = 0.011$ and $n_{fp} = 0.013$). The RMS errors, MAE, and coefficient r are provided in Table 4. While a large error is observed for the coarse mesh A, no improvement is brought by mesh C as compared to the results obtained using mesh B, on the contrary, the error increases as illustrated in Fig. 6b. According to Peyret and Taylor (1983), when the computational mesh is fine enough, all the dissipation scales and processes involved in the flow can be captured by simulations. If the mesh is further refined, energy dissipation increases, resulting in a slight decrease of the velocity and increase of the flow depth, as observed in Fig. 6a. This also suggests that the optimal value of C_s in the Smagorinsky model is linked to the mesh size.

Fig. 7 depicts the velocity and the RMS error corresponding to the simulations using best fit values of the bottom friction and of the non-dimensional coefficient C_s, all these values being optimized for the different mesh sizes (Table 5). Again, these optimized values are estimated by trial and error, in order to get the best fit with the data. It is clearly observed that the model reproduces very well the lateral distribution of depth-averaged velocity in comparison with the experimental data for both coarse and fine meshes. The greatest difference of flow depth that occurred in the case using the coarse mesh (mesh A), is only 0.047 cm (about 6.5% of observed flow depth). This value is 0.024 m/s (about 5.2% of cross-sectional average velocity U_0) for the RMS error of velocity (Table 5). However, using the very fine mesh C implies a significant increase in computational time due to the significant increase in the number of triangles. In addition, it could not improve the calculation results much for both flow depth and velocity.

As can be observed in Table 5, due to the change of mesh size and gradients of depth-averaged velocity (caused by changing the grid resolution), the non-dimensional coefficient C_s will increase significantly to maintain the same eddy viscosity if the mesh changes from the coarse mesh to the fine mesh. Therefore, both the non-dimensional coefficient C_s and Manning coefficient will change if the mesh of computational domain alters. The values of these parameters are, however, more or less the same if the meshes are fine enough.

The lateral distribution of the eddy viscosity ν_t is illustrated in Fig. 7b for the different mesh sizes, in the case of the optimized results. The distribution is quite irregular, and will be discussed in the next section. However, it can be observed that the magnitude of the eddy viscosity is greater in the case of the coarse mesh A, indicating that the lateral transfer of momentum needs to be increased in the computations to compensate for the increased numerical diffusion of the coarse mesh.

4.4. Eddy viscosity

Using mesh B, different models for determining the eddy viscosity ν_t are applied to investigate the influence of the choice of the turbulence closure model on the computational results: besides the Smagorinsky model, a constant value of ν_t, the simple model $\nu_t = \lambda u_* H$, and the one- and two-equation

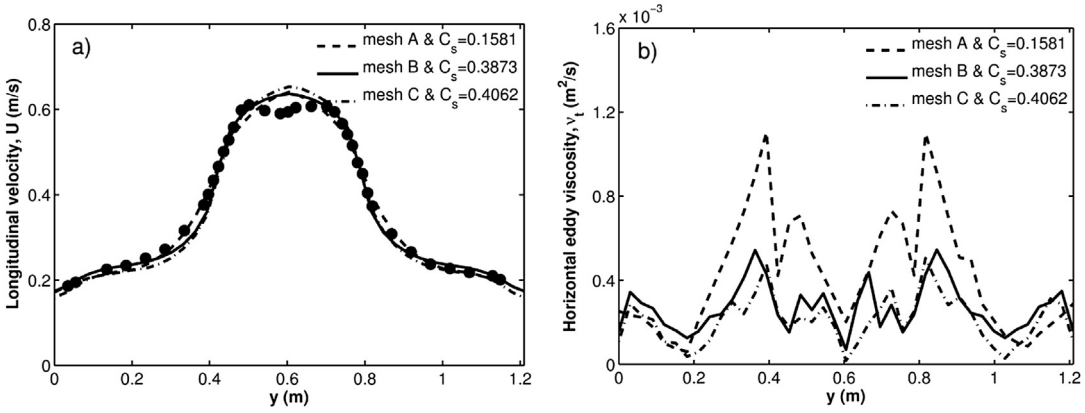

Fig. 7. Simulation result at the best approximate values of parameters in the cases using different meshes: a) lateral distribution of velocity and b) lateral distribution of eddy viscosity.

Table 5
Approximate value of parameters in the case using different meshes.

#	Eddy viscosity		Friction coefficient		Mesh	Flow depth, H (cm)		Longitudinal velocity		
	Model	C_s	n_{mc}	n_{fp}		Computed	Measured	RMS error	MAE	r
1	Smagorinsky turbulent model	0.1581	0.0098	0.0142	A	7.32	7.27	0.017	0.013	0.994
2		0.3873	0.011	0.013	B	7.27		0.016	0.012	0.995
3		0.4062	0.010	0.012	C	7.29		0.024	0.018	0.993

models are also used. The choice of the constant value of ν_t is made by calculating the average value of the eddy viscosity over the channel cross-section from the results obtained previously with the optimized Smagorinsky model ($C_s = 0.3873$, as illustrated in Fig. 7), leading to $\nu_t = 2.67 \cdot 10^{-4}$ m^2/s. For the case using the zero-equation turbulent model $\nu_t = \lambda u_* H$, one simulation was performed with $\lambda = 0.21$ in the whole channel while another was executed using $\lambda = 0.16$ for the main channel and $\lambda = 0.47$ in the floodplain region (Fraselle, 2010; Zeng et al., 2012). All simulations parameters are provided in Table 6. The velocities obtained from these simulations are compared to the experimental data and to the results achieved from the calibrated Smagorinsky turbulent model (Fig. 8). The detailed computed flow depth, RMS error of velocity, MAE, and coefficient r for all above calculation cases are given in Table 6.

All models provide similar results for both the flow depth and the velocity (Table 6) that are very close to the measurement value while the RMS error of velocity is only about 0.04 m/s (8.8% of cross-sectional average velocity U_0). In addition, these models produce very well the velocity within the main channel region in comparison to the experimental data.

However, looking closely at the results, a slightly better agreement between measurement data and calculated velocity is achieved both in the floodplains and in the main channel with the Smagorinsky model (Fig. 8a). This suggests that in the channel regions where the slow flow occurs (e.g. floodplains), the variation of the eddy viscosity enables the simulation of the correct turbulent flow, resulting in a well predicted velocity field. In the fast flow region (i.e. main channel), the change of eddy viscosity will affect the magnitude of velocity, especially in the channel center. Moreover, using the Smagorinsky model for the eddy viscosity also results in a better reproduction of the velocity in the transition region between floodplain and main channel. This means that

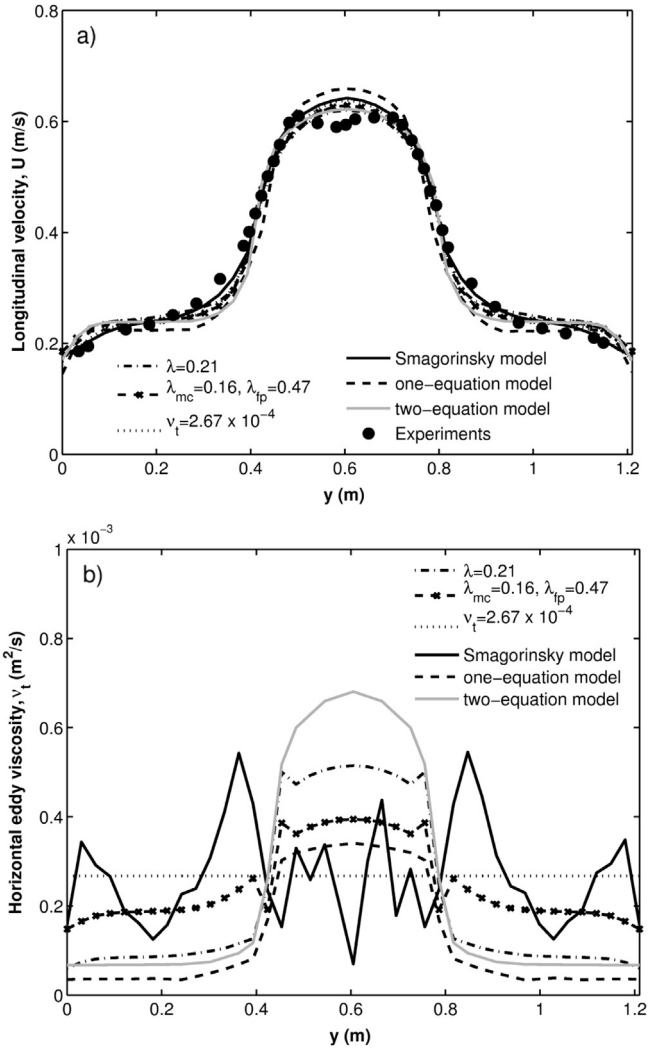

Fig. 8. Lateral distribution of: a) depth-averaged velocity and b) eddy viscosity obtained by using different models for eddy viscosity.

Table 6
Simulation results in the case using different models for eddy viscosity.

#	Eddy viscosity		Flow depth, H (cm)		Longitudinal velocity		
	Model	Value	Computed	Measured	RMS error	MAE	r
1	Constant	$\nu_t = 2.67 \times 10^{-4}$	7.28	7.27	0.021	0.018	0.991
2	$\nu_t = \lambda u_* h$	$\lambda = 0.21$	7.25		0.024	0.019	0.990
3		$\lambda_{mc} = 0.16$, $\lambda_{fp} = 0.47$	7.25		0.020	0.017	0.992
4	Smagorinsky turbulent model	$C_s = 0.3873$	7.27		0.016	0.012	0.995
5	One-equation model		7.30		0.040	0.033	0.977
6	Two-equation model		7.40		0.028	0.022	0.987

a good transverse transfer of momentum between the shallow and deep areas is obtained.

The magnitude of the eddy viscosity is of about 10^{-3} m^2/s as given in Fig. 8. This value is quite similar to the value reported by Wilson et al. (2002). They presented the eddy viscosity ν_t in a range between 10^{-4} and 10^{-3} m^2/s from their calculations using a $k-\varepsilon$ model in the framework of finite element Telemac-2D model. It is worth also to note that the use of a $k-\varepsilon$ model in this case did not provide any significant improvement compared to the other approaches.

Finally, Fig. 8b shows that the lateral distribution of the eddy viscosity varies significantly when using the Smagorinsky turbulent model, while the $\nu_t = \lambda u_* H$ model, the one- and two-equation models give much smoother results with a higher value in the main channel. The peak values of ν_t in the Smagorinsky model appear around the interface between main channel and floodplain where the large gradient of velocity occurs. The small values occur in the central channel and around the middle location of the floodplain where the maximum or a constant velocity happens.

5. Validation of the Smagorinsky approach

To further validate the applicability of the SLIM model with Smagorinsky turbulent closure to compound-channel flows, two additional simulations have been performed by using the remaining experiments reported in Section 3. It is worth noting that the mesh size and the value of the parameter C_s are kept the same as in Section 4 while the roughness coefficient changes depending on the experimental case.

5.1. Using the first experimental set-up

Fig. 9 shows the simulation result corresponding to the water discharge 0.015 m^3/s (No. 1 in Table 1) in the first experimental set-up of the Hydraulic Laboratory at UCL. Mesh B was used, and the bottom frictions for the main channel and floodplain are respectively 0.011 and 0.013, corresponding to the values calibrated in Section 4. A very good agreement between computed and measured velocities is obtained in the main channel while an overestimation of the calculated velocity is achieved in the floodplain regions. The RMS error of velocity is 0.026 m/s (corresponding to 6.3% of cross-sectional average velocity U_0) whiles the values of MAE and r are 0.021 m/s and 0.996, respectively. In addition, the calculated flow depth is 6.58 cm which is very close to the measurement value of 6.60 cm.

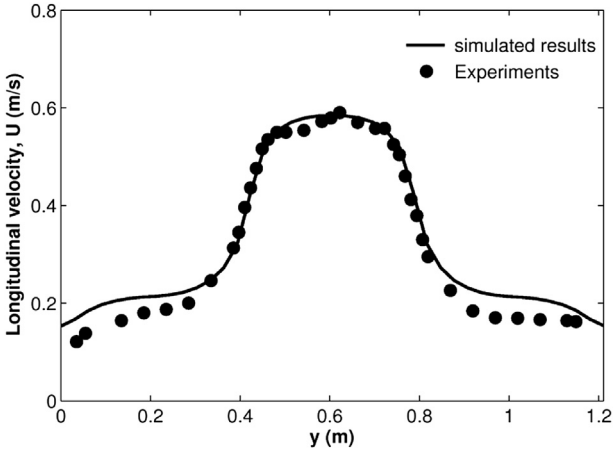

Fig. 9. Simulated and measured velocity for the water discharge of 0.015 m^3/s in the first experimental set-up.

Fig. 10 illustrates the lateral distribution of the depth-averaged velocity at different locations along the channel (e.g. x = 1.0 m, 2.0 m, …, 9.0 m) and the spatial variation of the eddy viscosity over the computational mesh in the channel. The velocity field is identical at the different locations, corresponding to a uniform flow as expected. The largest value of the velocity occurs in the deep flow area (main channel) with the maximum value of about 0.6 m/s at channel center while the smaller values appear in the shallow regions on the floodplains. The eddy viscosity varies significantly over the channel section, as already illustrated in Fig. 8b. The general trend of eddy viscosity is that the smaller value of eddy viscosity occurs around middle location of floodplain and in the channel center while the larger value appears in the transition area between these regions. It can be observed that with the Smagorinsky model, the computed eddy viscosity presents larger values at the transition between main channel and floodplain. This can be related to expression (3) where the value of the eddy viscosity coefficient depends on the velocity gradients that are higher in the transition zone between main channel and floodplain. So, the more important the velocity gradient, the more important the turbulent exchanges between the main channel and floodplain flows.

When the flow depth is low, the bed shear stress can increase sufficiently when using the Manning formula. This could be the reason why the computed velocity in the floodplain is larger than the observed data in this case.

5.2. Using second experimental set-up data

The second experimental data set reported in Zeng et al. (2012) was performed additionally in order to compare the lateral variation of eddy viscosity using the Smagorinsky turbulent model and $\nu_t = \overline{u'v'}/(\partial u/\partial x)$. The roughness coefficients (n_{mc} = 0.009 and n_{fp} = 0.02) are chosen as exactly the same values presented in Zeng et al. (2012) in which Manning's formula and the median particle diameter were used for estimating the Manning's coefficients of the main channel and the floodplain regions, respectively. In addition, the mesh of the channel employed is similar to mesh B, used in the first experiment.

Zeng et al. (2012) also provide an estimate of the eddy viscosity in the channel cross-section, obtained from the measured instantaneous and time averaged velocity in both longitudinal and transverse directions. First, the depth-averaged Reynolds' stresses $\tau = \rho\overline{u'v'}$ were calculated from the instantaneous velocities. Secondly, the transverse gradient of the longitudinal velocity $\partial u/\partial y$ was estimated and then, in

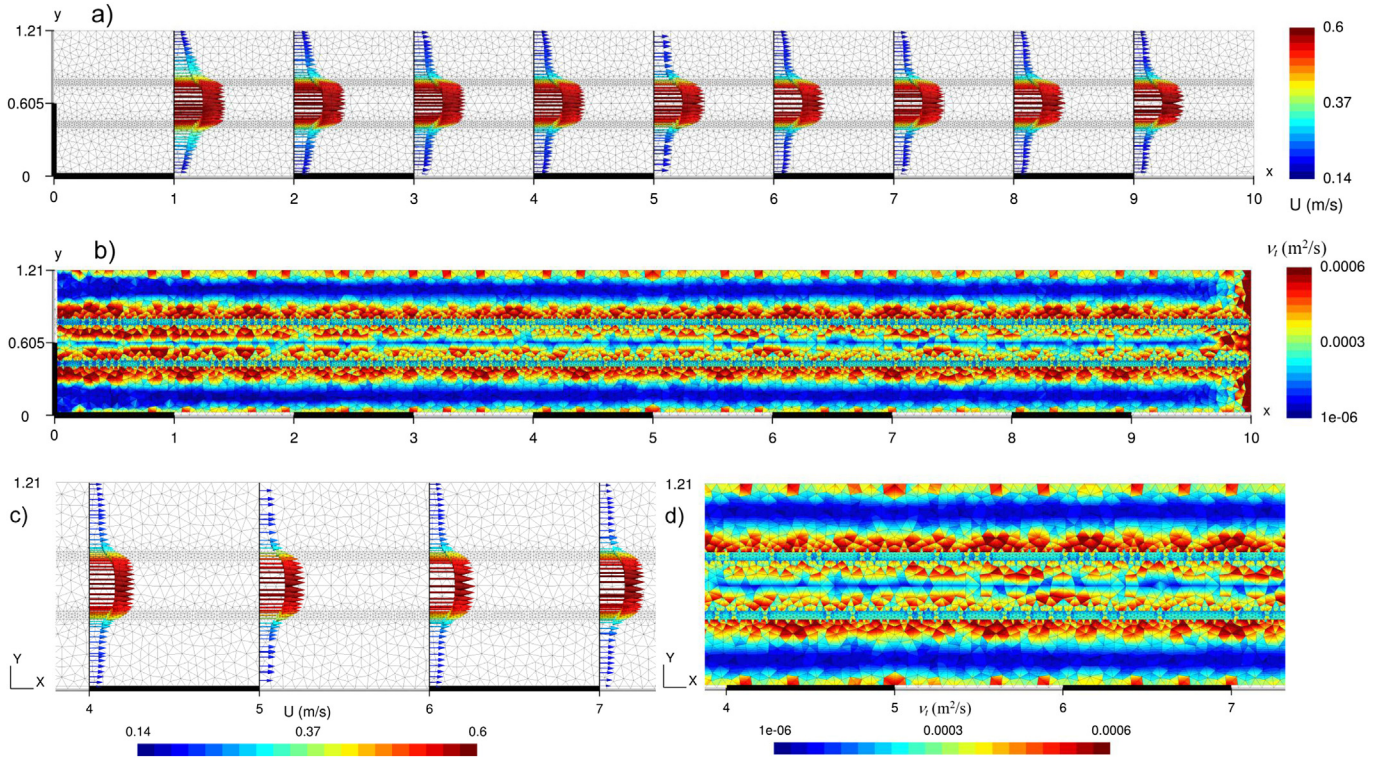

Fig. 10. Simulation results for the case using water discharge of 0.015 (m^3/s): a) velocity at different cross-sections in the channel, b) spatial distribution of eddy viscosity, c) closer view of velocity profile, and d) closer view of eddy viscosity.

the last step, the eddy viscosity coefficient was determined using the relationship

$$\nu_t = \frac{\overline{u'v'}}{\partial u/\partial y}. \tag{11}$$

The so-obtained experimental values of ν_t are used to compare with the predicted values.

As illustrated in Fig. 11a, similarly to the first experimental data set from UCL, the finite-element SLIM model reproduces well the flow dynamics, i.e. flow depth and lateral distribution of velocity in the channel. The flow depth is nearly uniform in the channel, with the computed value about 0.098 m, to be compared to the experimental value of 0.0972 m. The RMS error for the velocity is about 0.022 m/s (about 7.0% of cross-sectional average velocity U_0), presenting more or less similar RMS error of velocity as for the UCL test cases. The value of MAE is 0.018 and the coefficient r equals 0.986. In addition, a good agreement is also obtained for the velocity profile except in the central part of the channel where the computed profile overestimates the experimental data.

A comparison between the computed eddy viscosity and the experimental values in a half cross-section of the channel is given in Fig. 11b, presenting a very good agreement. It is clearly seen that both computed and measured values of eddy viscosity change rapidly in the transverse direction and the magnitude value is about 10^{-3} (m^2/s). Both model and experiment show that the maximum value of the eddy viscosity can be found around the interface between the floodplain and transition region. These results confirm again the validity of the Smagorinsky turbulent model in evaluating the eddy viscosity within compound open-channels in small-scale flume applications.

Fig. 12 shows the lateral distribution of depth-averaged velocity at different locations (e.g. x = 2.0, 4.0, 6.0, …, 18.0 m) and the spatial distribution of the eddy viscosity in the channel over the computational mesh. The computed velocity profiles in the cross-section are quite similar at different locations along the channel, revealing that the steady free surface flow was well represented by the model. The trend for the eddy viscosity is quite similar to those in the first experiment.

6. Summary and conclusion

The 2D depth averaged finite-element SLIM model (Second-generation Louvain-la-Neuve Ice-ocean Model), initially developed for ocean and estuarine applications, has been successfully applied to reproduce the steady free surface flow in compound open-channels. The aims of the study were (i) to demonstrate the capability of the SLIM model with a Smagorinsky turbulence closure model to reproduce the particular velocity distribution of such flows and (ii) to represent the small-scale variation of eddy viscosity in the channel section. The numerical simulations were calibrated using one experimental data set, and validated using two additional sets of data sets. A sensitivity analysis was carried out by varying the turbulence model for determining the eddy viscosity, the roughness coefficient, and the mesh refinement or grid resolution. Five different models or options including a constant

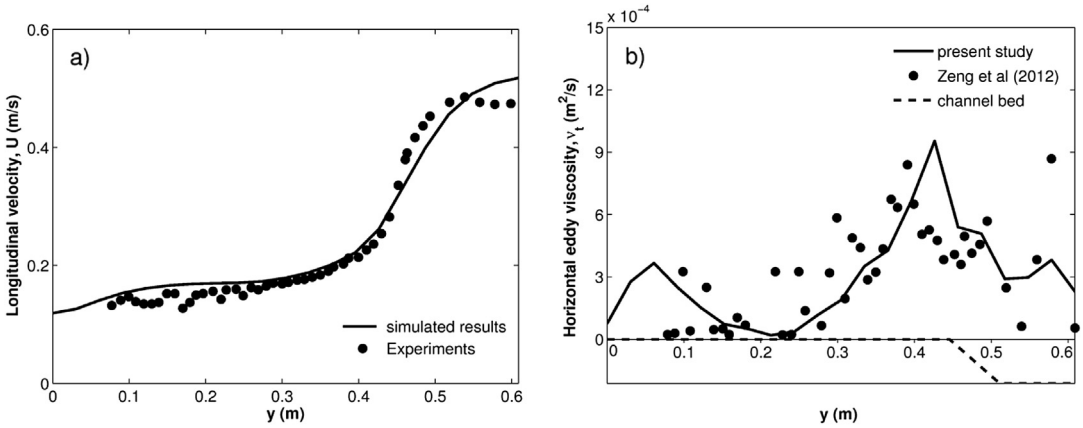

Fig. 11. Simulation results and observed data for the second experimental set-up, depth-averaged of: a) velocity and b) eddy viscosity.

value, zero-equation turbulent model with constant and variable value of non-dimensional eddy viscosity coefficient, one-equation model, two-equation model, and the Smagorinsky turbulent model for determining eddy viscosity coefficient were considered and compared to investigate the spatial variability of eddy viscosity in the channel section.

The Smagorinsky turbulent model which accounts for the effects of small-scale turbulent flow by using local subgrid-scale in evaluating the eddy viscosity is finally proved to be well adapted, providing even better results than the other more classical approaches considered. This model also represented very well the lateral variation of eddy viscosity in comparison with the measurement data obtained by using the depth-averaged Reynolds' stress and the lateral gradient of longitudinal velocity reported by Zeng et al. (2012). In the channel section, the small values of eddy viscosity occurred around the middle location of floodplains and central channel while the large values appeared around the transition locations between the main channel and floodplain. This variation of eddy viscosity allowed a better representation of turbulence flow and non-uniform velocity, especially in the region where the channel bed changes significantly. Another advantage of the Smagorinsky model is that only one parameter has to be adjusted which makes it quite simple and a useful tool for practical applications.

This study presents the first application of the finite-element SLIM model to a small-scale laboratory flow. Further developments will mainly concern the modeling of the effects secondary flows to make the model suitable to meandering channels. Although in the particular application presented here, no significant advantage is brought by using the more complicated models such as one- and two-equation turbulence models. The more application of such complex turbulence closure models in SLIM is also foreseen in the future to further enlarge the range of application of the model.

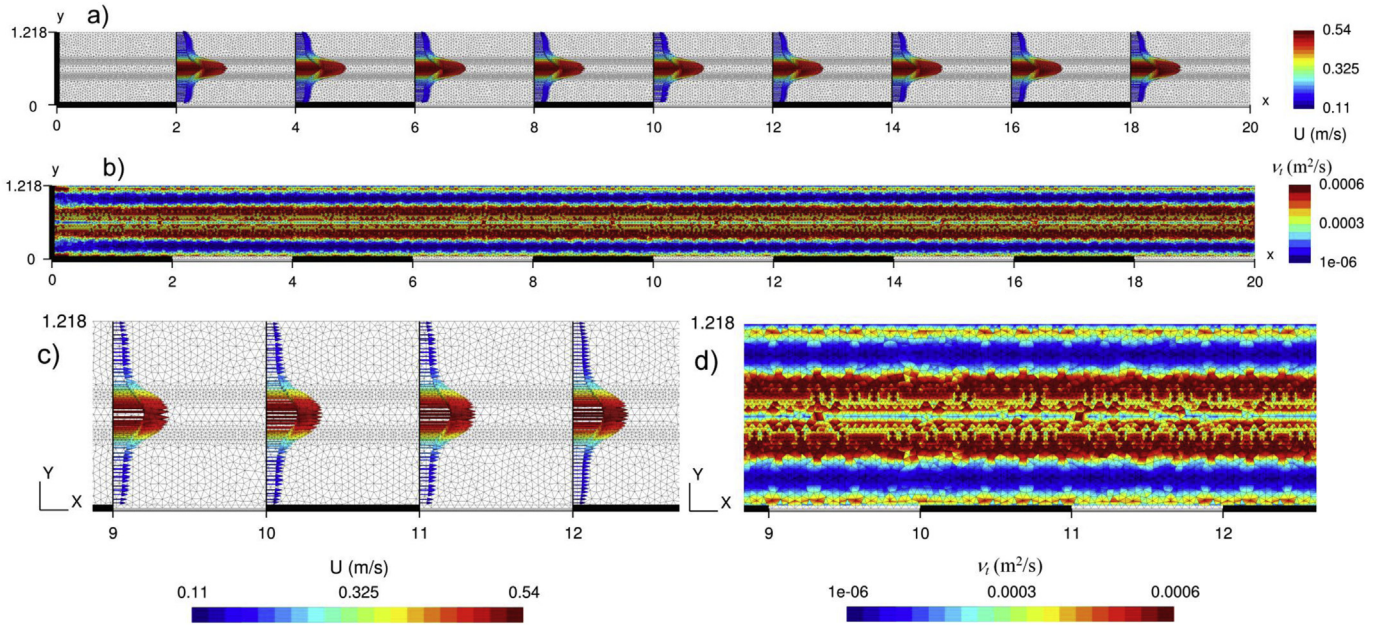

Fig. 12. Simulation results for the second experimental set-up: a) lateral distribution of velocity at different channel sections, b) spatial distribution of eddy viscosity in the whole channel, c) closer view of velocity profile, and d) closer view of eddy viscosity.

Acknowledgment

The present study was carried out in the framework of the project "Taking up the challenges of multi-scale marine modeling" which is funded by the Communauté Francaise de Belgique under contract ARC 10/15-028 (Actions de Recherche Concertées) with the aim of developing and using SLIM (www.climate.be/slim). Sandra Soares-Frazão and Eric Deleersnijder are honorary research associates with the Belgian National Fund for Scientific Research (F.R.S-FNRS). The authors would like to thank every member of the SLIM team for his/her contribution to the development of the model that was used in this study. Our thanks also go to Quentin Fraselle for sharing the measurement data used for the numerical simulations herein. We also would like to express our deep thanks to two anonymous reviewers for their useful comments and suggestions with constructive criticism that have helped improve the draft of this paper.

References

Bernard, P.-E., Chevaugeon, N., Legat, V., Deleersnijder, E., Remacle, J.-F., 2007. High-order h-adaptive discontinuous Galerkin methods for ocean modeling. Ocean Dyn. 57, 109–121 (+Erratum, 2007, 57, 579–580).

Bousmar, D., Rivière, N., Proust, S., Paquier, A., Morel, R., Zech, Y., 2005. Upstream discharge distribution in compound-channel flumes. J. Hydraul. Eng. 131 (5), 408–412.

Comblen, R., Lambrechts, J., Remacle, J.-F., Legat, V., 2010. Practical evaluation of five partly discontinuous finite element pairs for the non-conservative shallow water equations. Int. J. Numer. Methods Fluids 63, 701–724.

Darby, S.E., Thorne, C.R., 1996. Predicting stage-discharge curves in channels with bank vegetation. J. Hydraul. Eng. 122 (10), 583–586.

de Brye, B., de Brauwere, A., Gourgue, O., Kärnä, T., Lambrechts, J., Comblen, R., Deleersnijder, E., 2010. A finite-element, multi-scale model of the Scheldt tributaries, river, estuary and ROFI. Coast. Eng. 57, 850–863.

de Brye, B., Schellen, S., Sassi, M., Vermeulen, B.K.T., Deleersnijder, E., Hoitink, T., 2011. Preliminary results of a finite-element, multi-scale model of the Mahakam Delta (Indonesia). Ocean Dyn. 61, 1107–1120.

Ervine, D.A., Babaeyan-Koopaei, K., Sellin, R.H.J., 2000. Two-dimensional solution for straight and meandering overbank flows. J. Hydraul. Eng. 126 (9), 653–669.

Fraselle, Q., 2010. Solid Transport in Floodling Rivers with Deposition on the Floodplain: Experimental and Numerical Investigations (Ph.D. thesis). Université Catholique de Louvain, Louvain-la-Neuve, Belgium.

Geuzaine, C., Remacle, J.-F., 2009. GMSH: a finite element mesh generator with built-in pre-and post-processing facilities. Int. J. Numer. Method Eng. 79 (11), 1309–1331.

Joung, Y., Choi, S.-U., 2008. Investigation of twin vortices near the interface in turbulent compound open-channel flows using DNS data. J. Hydraul. Eng. 134 (12), 1744–1756.

Kärnä, T., de Brye, B., Gourgue, O., Lambrechts, J., Comblen, R., Legat, V., Deleersnijder, E., 2011. A fully implicit wetting–drying method for DG-FEM shallow water models, with an application to the Scheldt Estuary. Comput. Methods Appl. Mech. Eng. 200, 509–524.

Keller, R.J., Rodi, W., 1988. Prediction of flow characteristics in main channel/flood plain flows. J. Hydraul. Res. 26 (4), 425–441.

Kuzmin, D., Mierka, O., 2006. On the implementation of the k-ε turbulence model in incompressible flow solvers based on a finite element discretization. In: International Conference on Boundary and Interior Layers. Bail, Germany, pp. 1–8.

Lambrechts, J., Comblen, R., Legat, V., Geuzaine, C., Remacle, J.-F., 2008a. Multiscale mesh generation on the sphere. Ocean Dyn. 58, 461–473.

Lambrechts, J., Hanert, E., Deleersnijder, E., Bernard, P.-E., Legat, V., Remacle, J.-F., Wolanski, E., 2008b. A multi-scale model of the hydrodynamics of the whole Great Barrier Reef. Estuar. Coast. Shelf Sci. 79, 143–151.

Launder, B.E., Spalding, D.B., 1974. The numerical computation of turbulent flow. Comput. Method Appl. Mech. Eng. 3, 264–289.

Madsen, P.A., Rugbjerg, M., Warren, I.R., 1988. Subgrid modelling in depth integrated flows. In: Coastal Engineering Conference. Malaga, Spain, pp. 505–511.

Nadaoka, K., Yagi, H., 1998. Shallow-water turbulence modeling and horizontal large-eddy computation of river flow. J. Hydraul. Eng. 124 (5), 493–500.

Nasermoaddeli, M.H., Pasche, E., 2010. Modelling of undercutting and failure of non-cohesive river banks. In: Proceeding of River Flow 2010 International Conference on Fluvial Hydraulic. Braunschweig, Germany, pp. 1323–1330.

Pasche, E.R.G., Evers, P., 1985. Flow in compound channels with extreme flood plain roughness. In: Proceedings of the 21st IAHR Congress. Melbourne, Australia, pp. 384–389.

Peyret, R., Taylor, T.D., 1983. Computational Methods for Fluid Flow. Springer-Verlag, New York.

Pope, S.B., 2000. Turbulent Flows. Cambridge University Press.

Radojkovic, M., Djordjevic, S., 1985. Computation of discharge distribution in compound channels. In: Proceedings of the 21st IAHR Congress. Melbourne, Australia, pp. 367–371.

Rajaratnam, N., Ahmadi, R., 1981. Hydraulics of channels with flood-plains. J. Hydraul. Res. 19 (1), 43–60.

Rastogi, A.K., Rodi, W., 1978. Predictions of heat and mass transfer in open channels. J. Hydraul. Div. 104 (3), 397–420.

Rodi, W., 1980. Turbulence Models and Their Application in Hydraulics: a State of the Art Review. IAHR Book Publications, Delft.

Sellin, R.H.J., 1964. A laboratory investigation into the interaction between the flow in the channel of a river and that over its flood plain. Houille Blanche 7, 793–802.

Shiono, K., Knight, D.W., 1991. Turbulent open channel flows with variable depth across the channel. J. Fluid Mech. 222, 617–646.

Smagorinsky, J., 1963. General circulation experiments with the primitive equations. Mon. Weather Rev. 91, 99–164.

Smith, T.J., Takhar, H.S., Nov 1977. The Calculation of Oscillatory Flow in Open Channels using Mean Turbulence Energy Models. Unpublished report. Simon Engineering Labs, University of Manchester.

Sung-Uk, C., Pham Van, C., 2010. Impact of floodplain vegetation on the morphological change in the straight compound open-channel flow. In: Proceeding of International Symposium on Ecohydraulic 2010. Seoul, Korea, pp. 2217–2224.

Vionnet, C.A., Tassi, P.A., Martin Vide, J.P., 2004. Estimates of flow resistance and eddy viscosity coefficients for 2D modelling on vegetated floodplains. Hydrol. Process. 18, 2907–2926.

Vreugdenhil, C.B., Wijbenga, J.H.A., 1982. Computation of flow patterns in rivers. J. Hydraul. Div. 108 (11), 1296–1310.

Wark, J.B., Samuels, P.G., Ervine, D.A., 1990. A practical method of estimating velocity and discharge in a compound channel. In: White, W.R. (Ed.), River Flood Hydraulics. John Wiley & Sons, Inc., Chichester, UK, pp. 163–172.

Wilson, C.A.M.E., Bates, P.D., Hervouet, J.-M., 2002. Comparison of turbulence models for stage-discharge rating curve prediction in reach-scale compound channel flows using two-dimensional finite element methods. J. Hydrol. 257, 42–58.

Wormleaton, P.R., 1988. Determination of discharge in compound channels using the dynamic equation for lateral velocity distribution. In: Proceeding of International Conference on Fluvial Hydraulic, pp. 98–103.

Zeng, Y.H., Guymer, I., Spence, K.J., Huai, W.X., 2012. Application of analytical solutions in trapezoidal compound channel flow. River Res. Appl. 28 (1), 53–61.